Talanta 86 (2011) 337–348

Contents lists available at SciVerse ScienceDirect

Talanta

journal homepage: www.elsevier.com/locate/talanta

Development of phosphonate modified $Fe_{(1-x)}Mn_xFe_2O_4$ mixed ferrite nanoparticles: Novel peroxidase mimetics in enzyme linked immunosorbent assay

Dipsikha Bhattacharya[a], Ananya Baksi[a], Indranil Banerjee[b], Rajakumar Ananthakrishnan[a], Tapas K. Maiti[b], Panchanan Pramanik[a,*]

[a] Department of Chemistry, Indian Institute of Technology, Kharagpur 721302, India
[b] Department of Biotechnology, Indian Institute of Technology, Kharagpur 721302, India

ARTICLE INFO

Article history:
Received 24 June 2011
Received in revised form 26 August 2011
Accepted 14 September 2011
Available online 19 September 2011

Keywords:
PMIDA
ELISA
IgG
HRP
Bioassays

ABSTRACT

A highly facile and feasible strategy on the fabrication of advanced intrinsic peroxidase mimetics based on Mn^{2+} doped mixed ferrite ($Mn^{II}{}_xFe^{II}{}_{1-x}Fe^{III}{}_2O_4$) nanoparticles was demonstrated for the quantitative and sensitive detection of mouse IgG (as a model analyte). Mn^{2+} doped $Fe_{1-x}Mn_xFe_2O_4$ nanoparticles were synthesized using varying ratios of Mn^{2+}:Fe^{2+} ions and characterized by the well known complementary techniques. The increase of Mn^{2+} proportion had remarkably enhanced the peroxidase activity and magnetism. The catalytic activity of mixed ferrites was found to follow Michaelis–Menten kinetics and was noticeably higher than native Fe_3O_4. The calculated K_m and K_{cat} exhibited strong affinity with substrates which were remarkably higher than similar sized native magnetite nanoparticles and horseradish peroxidase (HRP). These findings stimulated us to develop carboxyl modified $Fe_{1-x}Mn_xFe_2O_4$ nanoparticles using phosphonomethyl immunodiacetic acid (PMIDA) to engineer PMIDA–$Fe_{1-x}Mn_xFe_2O_4$ fabricated enzyme linked immunosorbent assay (ELISA). Results of both PMIDA–$Fe_{1-x}Mn_xFe_2O_4$ linked ELISA revealed that the enhancements in absorbance during the catalysis of enzyme substrate were linearly proportional to the concentration of mouse IgG within the range between 0.1 μg/ml and 2.5 μg/ml. Further, this detection was ten times lower than previous reports and the detection limit of mouse IgG was 0.1 μg/ml. The advantages of our fabricated artificial peroxidase mimetics are combined of low cost, easy to prepare, better stability and tunable catalytic activity. Moreover, this method provides a new horizon for the development of promising analytical tools in the application of biocatalysis, bioassays, and bioseparation.

1. Introduction

Natural enzymes, due to high substrate specificity and high efficiency under mild conditions, have significant practical applications as biological catalysts in medicine, chemical industry, food processing and agriculture. However, they also have some intrinsic drawbacks such as dependence of catalytic activity on environmental conditions, time-consuming, expensive preparation as well as purification, low stability due to denaturation and digestion. These drawbacks have pushed the scientists to fabricate enzyme mimetics.

Encouraged by the multifaceted applications of nanomaterials, ongoing efforts are in roads to fabricate enzyme mimetics using designed nanostructures, which exhibit enzyme mimicking property along with stability and robustness to environmental conditions. Magnetic iron oxide nanoparticles (MNPs) have attracted increasing prospects, mainly in the biomedical field, including magnetic resonance imaging (MRI) [1–6], protein isolation and purification [7,8], magnetic targeting and drug delivery [9,10], cancer hyperthermia [11,12] and so on. Of late, it was reported that iron oxide nanoparticles have unexpected intrinsic-peroxidase like enzyme mimicking activity, which paves the way of nanoparticles as enzyme mimetics [13,14]. This surprising finding makes the magnetic Fe_3O_4 NPs as a benign artificial peroxidase combined with capture, separation and detection property. The peroxidase-like activity originates mainly from the heterogeneous Fenton-like catalytic activity of ferrous ions at the surface of Fe_3O_4 NPs [13]. These peroxidase-like activities have instigated scientists of replacing magnetic nanoparticles (MNPs) over horseradish peroxidase (HRP) in the traditional enzyme linked immunosorbent assay (ELISA) [15–19]. The advantages of substituting magnetic nanoparticles

* Corresponding author. Tel.: +91 3222 255221; fax: +91 3222 255303.
E-mail addresses: dipsikha.chem@gmail.com (D. Bhattacharya), pramanik1946@gmail.com (P. Pramanik).

0039-9140/$ – see front matter © 2011 Elsevier B.V. All rights reserved.
doi:10.1016/j.talanta.2011.09.026

concerns with its explicit superiority regarding the consistent activity over wide ranges of temperature, pHs and it can be readily synthesized in mass yield with relatively low cost [20–24]. However, it has been noticed that magnetite nanoparticles (MNPs) are still facing a challenge because of their lower stability and higher oxidizability, which hinders the peroxidase like activity of nanoparticles. Therefore, the attempts for the fabrication of better artificial peroxidase are on uprising, which can not only preserve its strong superparamagnetism but also can improve its catalytic activity.

Concurrently, many groups have demonstrated their efforts on the development of improved peroxidase mimicking Fenton like systems utilizing heterogeneous iron oxide nanoparticles either by optimizing their affinity towards substrates. This affinity could be enhanced by increasing electrostatic interaction between substrates and the nanoparticle surfaces or by introducing transition metal ions into the nanoparticle structure [24,25]. Recently, Gu et al. established a Prussian blue modified Fe_2O_3 nanoparticles with excellent electrochemical stability and higher catalytic activities arising from the electrostatic attraction between the positively charged substrate (TMB) and the negatively charged NPs [26]. Furthermore, some improved heterogeneous Fenton systems have been developed using Co(II) and Mn(II) ions as replacements of Fe(II) into magnetite $(Fe^{3+})[Fe^{2+}Fe^{3+}]O_4$ structure that may strongly promote the oxidative degradation of organic dyes in the presence of H_2O_2 [27]. It can be envisaged that the higher activity of these Mn and Co (M^{2+}) doped mixed ferrites compared to Fe_3O_4 was due to the one electron transfer exhibiting by the thermodynamically favorable reduction of $M_{surf}{}^{3+}$ (Co^{3+} and Mn^{3+}) by $Fe_{magnetite}{}^{2+}$ regenerating the active species M^{2+} (Co^{2+} and Mn^{2+}) [27,28]. Very recently, oxidative degradation of methyl orange in the presence of H_2O_2 was demonstrated using fabricated Fe_2MO_4 (M: Fe, Mn) activated carbons [29]. The incorporation of V and Ti into $Fe_{3-x}Ti_xO_4$ and $Fe_{3-x}V_xO_4$ nanostructures had prompted the adsorption as well as oxidative degradation of methylene blue (MB) in the presence of H_2O_2 [30,31].

It is also a well-established fact that manganese (II) complexes have been attracted considerable interest in the oxidative degradation of aromatic azo compounds in the presence of H_2O_2 [32,33]. There is scanty literature on the oxidative degradation of herbicide exploiting the peroxidase activity of Mn^{2+} ions in the presence of H_2O_2 [34]. It was assumed the peroxidase like activity of Mn^{2+} ions was aroused because of the Fenton like activity of Mn^{2+} ions in the presence of H_2O_2.

Our aim is to exploit the higher peroxidase activity of Mn^{2+} ions by fabricating a series of novel Mn doped mixed ferrite ($Mn^{II}{}_xFe^{II}{}_{1-x}Fe^{III}{}_2O_4$) nanoparticles, which are expected to show enhanced intrinsic peroxidase activity than previously investigated Fe_3O_4 nanoparticles. In this contribution, we proposed an efficient, facile and cost effective method of fabricating peroxidase mimetics $Mn^{II}{}_xFe^{II}{}_{1-x}Fe^{III}{}_2O_4$ nanoparticles: excellent enzyme mimics as a replacement of HRP used in conventional ELISA. It was observed that our synthesized $Mn^{II}{}_xFe^{II}{}_{1-x}Fe^{III}{}_2O_4$ nanoparticles showing better catalytic activities followed typical Michaelis–Menten kinetics. The observed K_m and K_{cat} values from these $Mn^{II}{}_xFe^{II}{}_{1-x}Fe^{III}{}_2O_4$ nanoparticles demonstrated that these nanoparticles possess higher peroxidase like activity towards the organic dye compared to the native magnetite nanoparticles. This higher peroxidase activity of $Fe_{1-x}Mn_xFe_2O_4$ nanoparticles instigated us to fabricate carboxyl decorated $Fe_{1-x}Mn_xFe_2O_4$ nanoparticles using phosphonomethyl iminodiacetic acid (PMIDA), a small inexpensive coupling agent, to impart carboxyl functionalities for facile bioconjugation with antibody. By employing the higher peroxidase properties of the antibody-linked-PMIDA–$Mn^{II}{}_{0.5}Fe^{II}{}_{0.5}Fe^{III}{}_2O_4$, both direct and indirect immunosorbent assays are designed, using the mouse IgG as model analyte, to confirm its potential application in enzyme immunoassays. It was observed that the detection limit obtained in indirect ELISA using our antibody-linked-PMIDA–$Mn^{II}{}_{0.5}Fe^{II}{}_{0.5}Fe^{III}{}_2O_4$ nanoparticles was lowest (0.1 μg/ml) in comparison to previous reports [26,35]. Exploiting the higher magnetic property and specific antibody–antigen interactions, we have also pioneerly fabricated the magnetic biodetection as well as separation of FITC-rabbit-anti-goat IgG. To the best of our knowledge, till date no researchers have embarked on the development and evaluation of peroxidase mimicking property of $Mn^{II}{}_{0.5}Fe^{II}{}_{0.5}Fe^{III}{}_2O_4$ nanoparticles: an efficient catalyst exploited for the detection, separation as well as quantification of mouse IgG as a model analyte by this modified PMIDA–$Mn^{II}{}_{0.5}Fe^{II}{}_{0.5}Fe^{III}{}_2O_4$ linked immunoassay. In a nutshell, this method holds great promise in the field of sensitive biodetection, bioseparation as well as catalysis of analytes to near future.

2. Experimental

2.1. Chemicals

Ferric chlorides ($FeCl_3$), ferrous sulfate ($FeSO_4{\cdot}7H_2O$), manganese chloride ($MnCl_2{\cdot}4H_2O$) were obtained from Merck, Germany. Phosphonomethyl iminodiacetic acid (PMIDA), 1,10-P henanthroline, hydroxylamine-hydrochloride, N-hydroxyl-succinimide (NHS), 1-ethyl-3-(3-dimethylaminopropyl) carbodiimide hydrochloride (EDC), sodium bicarbonate ($NaHCO_3$), sodium carbonate (Na_2CO_3), sodium azide (NaN_3) and Tween-20 were purchased from Aldrich, USA. Na_2HPO_4, NaH_2PO_4 and NaCl were purchased from Merck, Germany. Bovine serum albumin (BSA), *Z*-morpholinoethanesulfonic acid (MES buffer), Tris buffer, hydrogen peroxide (H_2O_2) (30%), 3,3,5,5-tetramethylbenzidine (TMB), mouse IgG, goat antimouse IgG, rabbit anti goat IgG, rabbit anti goat IgG-FITC, rabbit anti human IgG-FITC conjugate were purchased from Sigma–Aldrich.

2.2. Synthesis of Fe_3O_4, $Fe_{1-x}Mn_xFe_2O_4$ and PMIDA modified $Fe_{1-x}Mn_xFe_2O_4$ nanoparticles

Superparamagnetic magnetite (Fe_3O_4) nanoparticles were prepared by controlled chemical co-precipitation of Fe^{2+} and Fe^{3+} (1:2 weight ratio) ratio from ammoniacal solution under argon atmosphere. Substituted ferrites ($Fe_{1-x}Mn_xFe_2O_4$) were prepared by similar co-precipitation technique in N_2 atmosphere using milli-Q water and ammonium hydroxide as a base [36]. For the synthesis of ($Fe_{0.5}Mn_{0.5}Fe_2O_4$) magnetic nanoparticles, 0.324 g of $FeCl_3$, 0.140 g of $FeSO_4{\cdot}7H_2O$ and 0.098 g of $MnCl_2{\cdot}4H_2O$ were taken in 40 ml of absolutely deoxygenated milli-Q water in a 100 ml three necked flask equipped with argon flow and a mechanical stirrer. 5 ml of NH_3 (25%) solution was added into it drop wise over a period of 15 min during which black precipitates were formed. The reaction mixture was then stirred for 2 h at 70 °C. After completion of the reaction, black particles were separated and washed 5 times with milli-Q water using magnetic concentrator. For the synthesis of ($Fe_{0.85}Mn_{0.15}Fe_2O_4$) nanoparticles, same procedure was repeated only the different amounts of reagents i.e. 0.320 g of $FeCl_3$, 0.236 g of $FeSO_4{\cdot}7H_2O$ and 0.030 g of $MnCl_2{\cdot}4H_2O$ were taken. For the surface modification of magnetic ferrofluid ($Fe_{0.5}Mn_{0.5}Fe_2O_4$) by PMIDA, mixed ferrite nanoparticles and PMIDA were taken in 1:2 molar ratio in an alkaline medium (pH 8–9). The solution was again sonicated for 20 min and magnetically stirred for 24 h. The particles were separated magnetically, and washed five times with water followed by ethanol and dried in vacuum. Few drops of the suspended particles in water were acidified with dilute acetic acid (pH was maintained 4–5) and further dispersed in 10 ml of millipore water by ultrasonication. The magnetic nanoparticles were recovered from the reaction mixture using a permanent magnet.

2.3. Kinetic analysis of peroxidase like mixed ferrite nanoparticles

The steady-state kinetic assays were performed at room temperature in a reaction system using 3.22×10^{-10} M of each Fe_3O_4, $Mn_{0.5}Fe_{0.5}Fe_2O_4$, and $Mn_{0.15}Fe_{0.85}Fe_2O_4$ nanoparticles in 1 ml of reaction buffer (0.1 M NaAc, pH 4) in the presence of H_2O_2 and TMB. The kinetic analysis of these nanoparticles with TMB as the substrate was performed by adding 0.8 M of H_2O_2 and different amounts (0–800 μM) of TMB solution. The kinetic analysis of these nanoparticles with H_2O_2 as the substrate was performed by adding 800 μM of TMB and different amounts (0–1.8 M) of 30% H_2O_2 solution. All the reactions were monitored in time scan mode at 652 nm using the Shimadzu UV 1700 spectrophotometer. Catalytic parameters were determined by fitting the absorbance data to the Michaelis–Menten equation (1). The apparent kinetic parameters were determined by fitting the absorbance data according to the Michaelis–Menten equation.

$$v = \frac{V_{max} \times [S]}{K_m + [S]} \quad (1)$$

The Michaelis–Menten equation describes the relationship between the rates of substrate conversion by an enzyme and the concentration of the substrate. In this equation, v is the rate of conversion, V_{max} is the maximum rate of conversion, [S] is the substrate concentration, and K_m is the Michaelis constant. The Michaelis constant is equivalent to the substrate concentration at which the rate of conversion is half of V_{max} and K_m approximates the affinity of the enzyme for the substrate.

2.4. Functionalization of PMIDA–$Mn_{0.5}Fe_{0.5}Fe_2O_4$ with antibody for implications in direct or indirect immunosorbent assay

The MNPs were functionalized with either goat antimouse IgG or rabbit anti goat IgG through the crosslinking between the free carboxylic groups on PMIDA–$Mn_{0.5}Fe_{0.5}Fe_2O_4$ nanoparticles with the available NH_2 groups of antibodies. Approximately 1 mg of PMIDA–$Mn_{0.5}Fe_{0.5}Fe_2O_4$ nanoparticles were suspended in 1 ml of 0.1 M MES buffer (pH 5.5). Aqueous solutions of 10 mM NHS and 4 mM of EDC dissolved in MES buffer were freshly prepared and 0.5 ml of each solution was immediately added to the solution. The nanoparticles were incubated at room temperature (RT) with gentle shaking. After 2 h, these nanoparticles were centrifuged and washed with 10 mM PBS (pH 7.4), and then resuspended in 1 ml PBS followed by the addition of 100 μl of either goat-antimouse or rabbit-antigoat antibody at a concentration of 5 mg/ml. The mixture was incubated at RT for 12 h with an end to end shaking. These nanoparticles were repeatedly washed with 10 mM PBS (pH 7.4) and resuspended in quenching solution [40 mM Tris–HCl with 0.05% BSA] for 1 h to block free carboxylic groups. Protein coated nanoparticles were purified by magnetic separation and resuspended in PBS (1 ml) with 1% BSA and stored at 4 °C until use.

2.5. Detection of mouse IgG as a model by both direct and indirect immunosorbent assay

The detection of mouse IgG using these antibody linked PMIDA–$Mn_{0.5}Fe_{0.5}Fe_2O_4$ nanoconjugates was studied by performing both direct and indirect immunoassay [35]. For direct ELISA, mouse IgG (0.2–2.5 μg/ml, total of six concentrations) was loaded into the wells of a 96-well microtiter plate in 0.1 M $NaHCO_3$ at 4 °C for overnight incubation. After the wells were washed with PBST (0.05% Tween 20 in PBS) and PBS for 3 times, 100 μl of 1% BSA in PBS was added to the wells and incubated for 2 h at 37 °C. The wells were then washed with PBST and PBS three times again. Then, 500 μg/ml goat-antimouse IgG (5 mg/ml) functionalized PMIDA–$Mn_{0.5}Fe_{0.5}Fe_2O_4$s in PBS was added (5 μg/100 μl) and incubated for 2 h at 37 °C. The wells were then washed with PBST 3 times, followed by a PBS wash. Afterward, 100 μl of reaction buffer (0.1 M NaAc, pH 4, 0.8 M of 30% H_2O_2, 800 μM TMB) was added into the wells. The absorbance of each well at 652 nm was measured using a microplate reader (SpectraMax M5, Molecular Device).

For detection of the mouse IgG by an indirect ELISA method, mouse IgG was first loaded into the wells from 0.1 μg/ml to 0.35 μg/ml. After rinsing with PBS, the wells were blocked by 1% BSA in PBS (100 μl in each well). Goat anti-mouse IgG was then added to the wells at a concentration of 100 ng/well and incubated for 2 h at 37 °C. Then, 100 μl solutions of rabbit anti goat-IgG linked PMIDA–$Mn_{0.5}Fe_{0.5}Fe_2O_4$s at a concentration of 500 μg/ml were added to each well at 5 μg/well concentration and the mixture was kept at 37 °C for 1 h. The wells were then washed with PBST three times and with PBS once. Reaction buffer (100 μl) containing TMB and H_2O_2 was added to each well, and absorbance at 652 nm was measured.

2.6. Bio-conjugation of PMIDA–$Mn_{0.5}Fe_{0.5}Fe_2O_4$s with goat IgG-Ag and magnetic separation of the target antibody

For the qualitative detection and magnetic bioseparation of the FITC labeled rabbit anti-goat IgG (FITC-rabbit anti-goat IgG, concentration 1 mg/ml), a solution of goat anti-mouse IgG-linked PMIDA–$Mn_{0.5}Fe_{0.5}Fe_2O_4$s (same procedure as reported in direct ELISA, 100 μl, 1 mg/ml) was incubated with a solution of FITC-antigoat IgG in PBS (100 μl, 1 mg/ml) with overnight shaking at RT [37]. The mixture was then thoroughly mixed and the fluorescence of the mixed solution (100 μl) was recorded immediately before magnetic separation. The FITC-anti-goat IgG-linked magnetic nanocomposites was separated by magnetic separation and washed with the PBS buffer solution (three times). The fluorescence of the nanocomposites solution and the supernatant were measured after magnetic separation. The selectivity of this magnetic separation method was accomplished by a control experiment with FITC-rabbit-anti human IgG, following the same protocol, described in the target experiment.

2.7. Instrumentation

The exact compositions of these nanoparticles were analyzed by the spectrophotometric determination of total Fe content and Fe(II) content using standard 1,10-phenanthroline and the Mn(II) content was back-calculated from the total Fe content and it was well matched with the exact amount of ions present in the nanoparticles. (Details of the characterizations were incorporated in Supporting Information.) The hydrodynamic size (HD) of the particle aggregates was measured by laser light scattering using a Brookhaven 90 Plus particle size analyzer. The surface charge of the nanoparticles was investigated through zeta potential 100 measurements (Zetasizer 4, Malvern Instruments, UK). The surface chemistry of the nanoparticles was performed by using a Thermo Nicolet Nexux FTIR model 870 spectrometer. The X-ray photoelectron spectroscopic (XPS) data was collected using an Al Ka excitation source in an ESCA-2000 Multilab apparatus (VG microtech). The catalytic properties of the synthesized nanoparticles for immunoassay applications were characterized by the color reaction of TMB with the presence of H_2O_2. For the UV–vis absorption measurements of the catalytic reaction, we used a Shimadzu absorption spectrophotometer (model no. UV-1700). For fluorescence measurement, a Spexfluorolog-3 spectrofluorimeter (model no. FL3-11) was used respectively. The phase analysis of the synthesized magnetite nanopowder was performed on an X'pert Pro Phillips X-ray diffractometer. The sample for XRD was prepared by the deposition of well dispersed nanoparticles on a glass slide and, after drying, the analysis was performed by using cobalt as the target material.

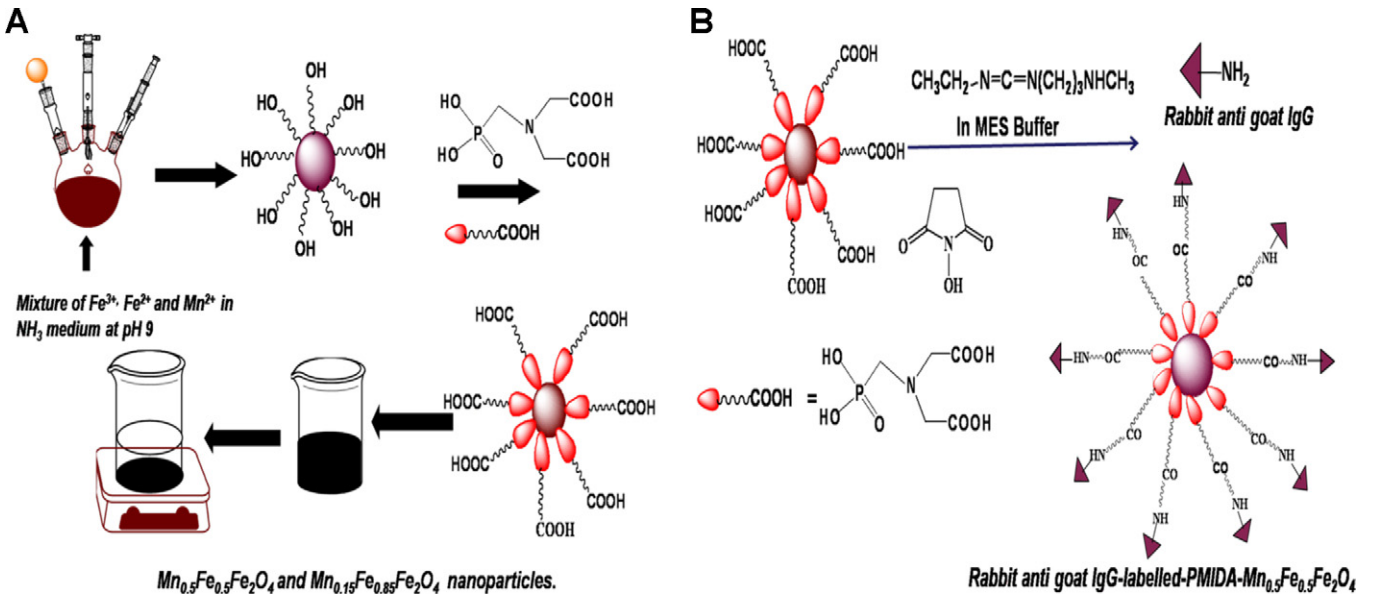

Scheme 1. Fabrication strategy of (A) PMIDA modified Mn^{2+} doped $Mn_{0.5}Fe_{0.5}Fe_2O_4$ nanoparticles and (B) antibody (rabbit anti-goat IgG/goat-IgG) immobilization of PMIDA–$Mn_{0.5}Fe_{0.5}Fe_2O_4$ nanoparticles by standard EDC/NHS chemistry for implications of MNP-ELISA.

High-resolution transmission electron microscopy (HRTEM) (JEOL 3010, Japan) was employed to characterize the microstructure of the nanoparticles at 200 kV. For direct and indirect ELISA as well as antibody quantification, the absorbance at each well at 652 nm was measured using a microplate reader.

3. Results and discussions

3.1. Synthesis of Mn^{2+} doped mixed ferrite nanoparticles ($Mn_xFe_{1-x}Fe_2O_4$)

Three types of nanoparticles (Fe_3O_4, $Mn^{II}_{0.15}Fe^{II}_{0.85}Fe^{III}_2O_4$ and $Mn^{II}_{0.5}Fe^{II}_{0.5}Fe^{III}_2O_4$) were fabricated with varying composition of Mn^{2+}:Fe^{2+} ions to develop the peroxidase mimetics. These nanoparticles were synthesized by co-precipitation method with varying ratio of Mn^{2+}: Fe^{2+} in NH_4OH solution at pH 9 under argon atmosphere [36]. The observed enhanced reactivity of the $Mn_xFe_{1-x}Fe_2O_4$ nanoparticles compared to Fe_3O_4 was speculated due to the combined peroxidase like activity of both surface active Fe^{2+} and Mn^{2+} atoms towards the decomposition of H_2O_2 [28,38]. As our aim was to exploit the increased peroxidase like activity to mimicking HRP in ELISA, the surface of $Mn^{II}_{0.5}Fe^{II}_{0.5}Fe^{III}_2O_4$ nanoparticles were further modified with PMIDA to generate active carboxyl functionalities for further bioconjugations to antibodies. The synthesis of $Mn^{II}_{0.5}Fe^{II}_{0.5}Fe^{III}_2O_4$ nanoparticles and the PMIDA modification strategy was shown in Scheme 1A. The phosphonate groups of PMIDA strongly anchored the nanoparticulate surface and the free carboxyl functions of PMIDA exposed on the surface of the nanoparticles. These free carboxyl functionalities induced electrostatic repulsion between the nanocrystals, developing a stable ferrofluid for further bioapplications. Different antibodies (goat-anti-mouse IgG and rabbit antigoat IgG) were conjugated on the surface of the PMIDA–$Mn^{II}_{0.5}Fe^{II}_{0.5}Fe^{III}_2O_4$ nanoparticles by the standard EDC/NHS protocol at pH 5, as observed in Scheme 1B. Initially, the carboxyl groups of PMIDA conjugated $Mn^{II}_{0.5}Fe^{II}_{0.5}Fe^{III}_2O_4$ nanoparticles were activated by incubating with EDC/NHS at pH 5 in MES buffer for 2 h. The available NH_2 groups of the anti-mouse IgG/rabbit antigoat IgGs were coupled with the activated carboxyl groups of PMIDA–$Mn^{II}_{0.5}Fe^{II}_{0.5}Fe^{III}_2O_4$ nanoparticles to fabricate the detection tool for mouse IgG detection by modified PMIDA–$Mn_{0.5}{}^{II}Fe^{II}_{0.5}Fe^{III}_2O_4$ linked immunosorbent assay (Scheme 2A).

In order to demonstrate their magnetic bio-separation and concentration implications in immunoassays, the PMIDA–$Mn^{II}_{0.5}Fe^{II}_{0.5}Fe^{III}_2O_4$ nanoparticles were bio-conjugated with goat-antimouse IgG to construct goat-IgG labeled PMIDA–$Mn^{II}_{0.5}Fe^{II}_{0.5}Fe^{III}_2O_4$ nanoparticles and then utilized in the magnetic separation of FITC-labeled rabbit anti-goat IgG antibody, according to the procedure shown in Scheme 2B.

3.2. Structural and compositional characterization of coated and uncoated ferrite nanoparticles

The XRD patterns of $Fe_{1-x}Mn_xFe_2O_4$ (x = 0.15 and 0.5) nanoparticles in Fig. 1 showed that all the ferrites synthesized were

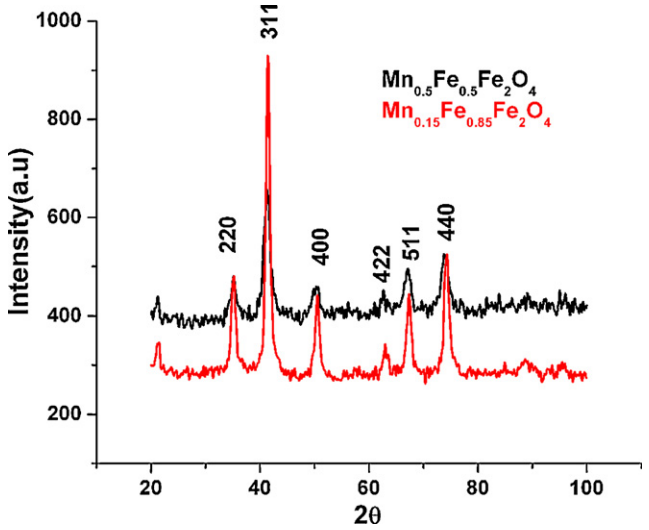

Fig. 1. XRD patterns of (A) $Fe_{0.5}Mn_{0.5}Fe_2O_4$, and (B) $Fe_{0.85}Mn_{0.15}Fe_2O_4$ nanoparticles.

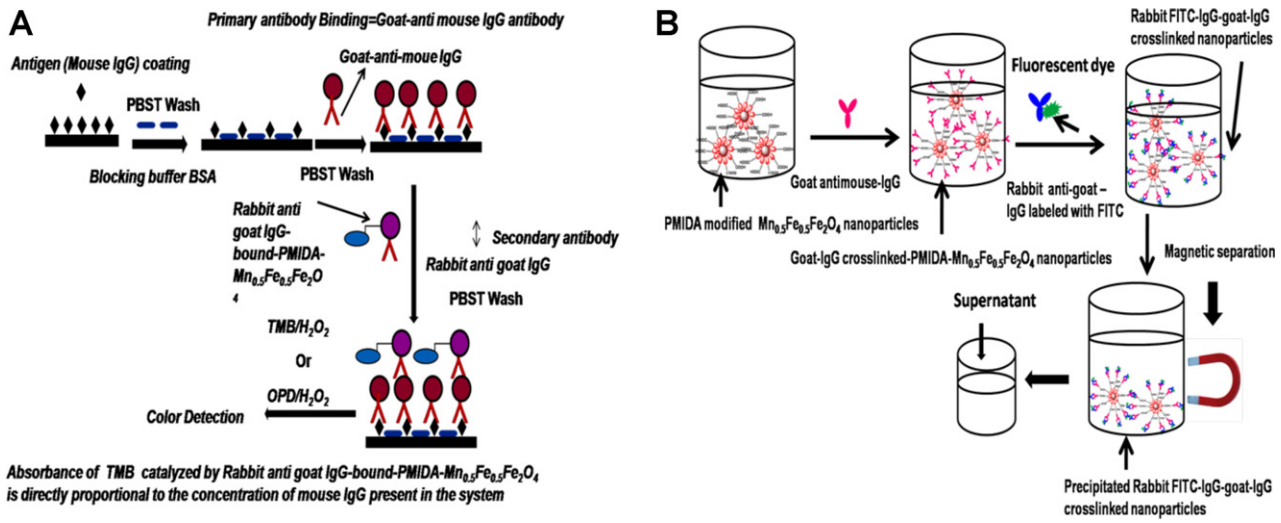

Scheme 2. (A) Schematic representation of the employed in PMIDA–$Mn_{0.5}Fe_{0.5}Fe_2O_4$-linked indirect immunosorbent assay. (B) Fabrication strategy of detection and magnetic bioseparation of FITC-rabbit-anti-goat-IgG using goat-IgG-PMIDA–$Mn_{0.5}Fe_{0.5}Fe_2O_4$ nanoparticles.

of single-phase cubic ferrite systems. The broadening of peaks indicated small crystalline sizes of the nanoparticles, which was translated into an average core size of about 8 nm using the Debye–Scherrer formula for spherical particles. The relatively low intensity and broadness of peaks produced were due to nanocrystallinity of the ferrite particles. The crystallite sizes of $Fe_{1-x}Mn_xFe_2O_4$ ($x = 0.15$ and 0.5) nanoparticles were calculated from the XRD line (3 1 1) broadening using Scherrer's formula.

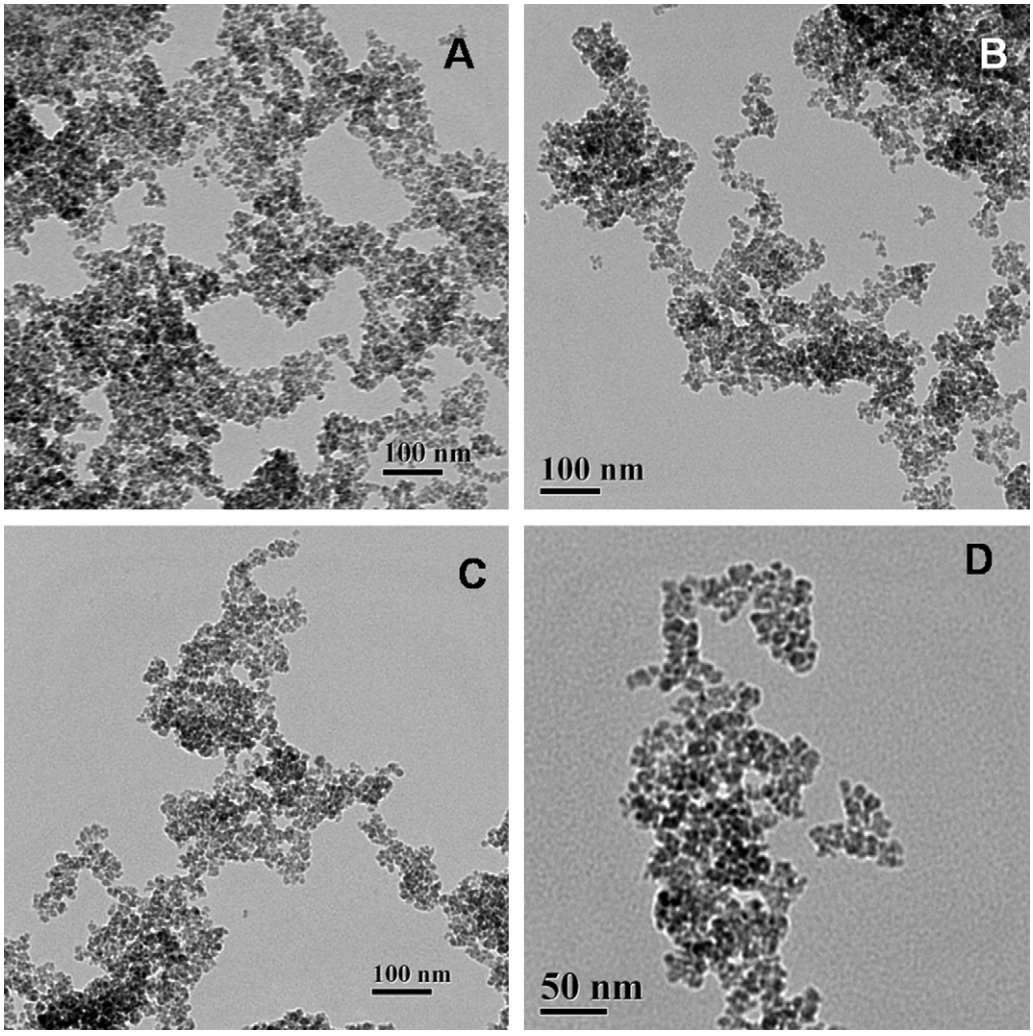

Fig. 2. Representative TEM micrographs of (A) $Fe_{0.5}Mn_{0.5}Fe_2O_4$, (B) $Fe_{0.85}Mn_{0.15}Fe_2O_4$, (C) PMIDA–$Fe_{0.5}Mn_{0.5}Fe_2O_4$, and (D) PMIDA–$Fe_{0.5}Mn_{0.5}Fe_2O_4$ in high resolution.

Table 1
Hydrodynamic (HD) size, PDI and zeta potential of the $Fe_{0.5}Mn_{0.5}Fe_2O_4$ and PMIDA–$Fe_{0.5}Mn_{0.5}Fe_2O_4$.

Nanoparticles (NPs)	HD size (nm) at pH 7	PDI	Zeta potential (mV) at pH 7	Zeta potential (mV) at pH 9	Zeta potential (mV) at pH 4
$Fe_{0.5}Mn_{0.5}Fe_2O_4$	450 nm	0.212	−7.6	−7.8	−7.6
PMIDA–$Fe_{0.5}Mn_{0.5}Fe_2O_4$ [2]	126 ± 9 nm	0.119	−37.6	−41.4	−32.3

It had been observed that the crystallite sizes of $Fe_{1-x}Mn_xFe_2O_4$ ferrite particles decreased from 10 to 8 nm with increased Mn^{2+} concentrations from 0.15 to 0.5 and this observation was similar as reported by Bahadur et al. [36] and Upadhayay et al. [39]. The representative TEM micrographs in Fig. 2 illustrated that the uncoated $Fe_{1-x}Mn_xFe_2O_4$ ($x = 0.5$ and 0.15) nanoparticles had a particle size in the range of 7–9 nm respectively with a high amount of agglomeration. After modification, the TEM images displayed that the size of the PMIDA–$Fe_{0.5}Mn_{0.5}Fe_2O_4$ (approximately 10–11 nm) somewhat increased than uncoated particles. This increase was due to the presence of adsorbed phosphonate layer on the mixed ferrite nanoparticles. These PMIDA modified nanoparticles displayed higher dispersibility in the aqueous medium due to the immense number of carboxyl groups on the surface and this dispersion remained stable for 1 month without any agglomeration. In contrast, the bare mixed ferrite nanoparticles exhibited rapid agglomeration after dispersing in aqueous medium and precipitated from the aqueous medium in less than 30 min (data not shown).

The average hydrodynamic diameters (HDs) of uncoated $Fe_{0.5}Mn_{0.5}Fe_2O_4$ and PMIDA–$Fe_{0.5}Mn_{0.5}Fe_2O_4$ nanoparticles were studied under different pH and the data was shown in Table 1. The HD sizes of PMIDA–$Fe_{0.5}Mn_{0.5}Fe_2O_4$ nanoparticles, observed in the range of 126–135 nm respectively at physiological pH, were considerably smaller than uncoated $Fe_{0.5}Mn_{0.5}Fe_2O_4$ (450 nm) one and the diameter of these PMIDA-modified nanoparticles was found to increase with decreasing pH. This increase might be attributed from the protonation on PMIDA-modified mixed ferrite nanoparticles at the lower range of pH. It was further observed that the corresponding zeta potentials of the nanoparticles (Table 1) were in good agreement with the dynamic laser light scattering (DLS) measurements. The zeta potential values of both bare-mixed ferrites and PMIDA modified mixed ferrites were observed at physiological pH. The uncoated mixed ferrite exhibited zeta potential value of −7.6 mV at pH 7 due to the surface hydroxyl groups on the ferrite surface, whereas PMIDA modified mixed ferrites displayed a higher zeta potential −37.8 mV at pH 7 and the value was observed increasing with increasing pH. This high negative surface charge at pH 7 confirmed the presence of carboxyl groups on the magnetite surface. On the contrary, the zeta potential value of modified nanoparticles showed a less negative surface charge at pH 4 due to the predominance of protonated carboxyl groups on the nanoparticle surface.

The FT-IR spectrums of bare $Fe_{0.5}Mn_{0.5}Fe_2O_4$ and PMIDA–$Fe_{0.5}Mn_{0.5}Fe_2O_4$ were illustrated in Fig. 3. For bare $Fe_{0.5}Mn_{0.5}Fe_2O_4$ nanoparticles, a strong band appeared at 584 cm^{-1} due to the presence of Fe–O vibration of magnetic core. Besides the presence of 584 cm^{-1} for Fe–O vibration, a broad band around 1180–1034 cm^{-1} appeared in PMIDA–$Fe_{0.5}Mn_{0.5}Fe_2O_4$ nanoparticles ascribing due to the presence of Fe–O–P and P=O stretching bands superimposed on one another. As compared to unbound PMIDA (S1), the peak associated with the C=O stretching bands of carboxylic acids around 1736 cm^{-1} in PMIDA (Supporting information S1) was shifted to 1624 cm^{-1} in PMIDA–$Fe_{0.5}Mn_{0.5}Fe_2O_4$, possibly due to the establishment of intraparticle hydrogen bonding between the surface $-CO_2H$ groups [40]. One very small peak compared to unbound PMIDA appeared at 1736 cm^{-1} which was due to the free CO_2H groups on the surface of the PMIDA–$Fe_{0.5}Mn_{0.5}Fe_2O_4$ nanoparticles.

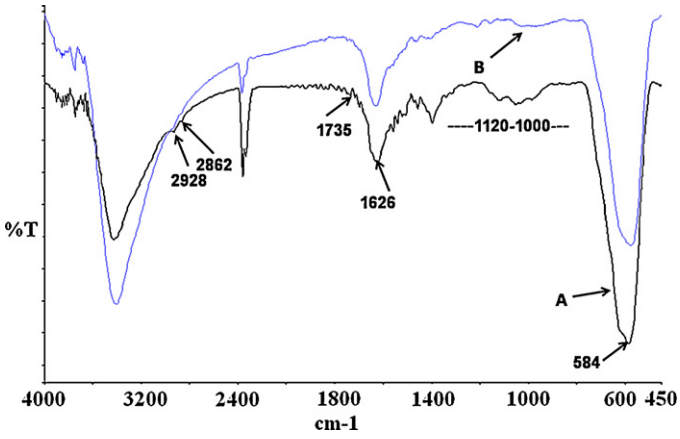

Fig. 3. FT-IR spectra of (A) PMIDA–$Fe_{0.5}Mn_{0.5}Fe_2O_4$ and (B) bare $Fe_{0.5}Mn_{0.5}Fe_2O_4$.

X-ray photoelectron spectroscopy analysis was further used to authenticate the successful modification with PMIDA on these mixed ferrite nanoparticles (Fig. 4A–E). The high-resolution C1s spectrum (Fig. 4A) displayed three peaks at 284.73, 284.5 and 288.14 eV, attributed to C–C, C–O and C=O (typical of ester/carboxylic acid). The Fe2p doublet with binding energy values of 710.8 and 724.29 eV (Fig. 4B) implied the presence of Fe–O bonds, typical for magnetite. The P2p spectrum (Fig. 4C) exhibited two peaks at 132.26 and 138.9 eV corresponding to $P2p_{3/2}$ and $P2p_{1/2}$, respectively. Furthermore, the high resolution O1s spectrum (Fig. 4D) of PMIDA-coated magnetite displayed peaks at 530.15, 530.1, 531.9, and 532.4 eV, which corresponded to presence of different oxygen atoms in four different environments as P–O, C–O, Fe–O, and O–H. The presence of Mn^{2+} was confirmed in this PMIDA–$Fe_{0.5}Mn_{0.5}Fe_2O_4$ by XPS analysis. The $Mn2p_{3/2}$ and $Mn2p_{1/2}$ doublet with binding energy values of 640.2 and 651.97 (Fig. 4E) validated the presence of Mn–O bonds in the sample [41].

3.3. Magnetism

Dopant dependent variation of magnetization of mixed ferrite nanoparticles was measured by vibration sample magnetometry (VSM) at room temperature. Fig. 5 showed variation of room temperature specific extent of magnetization of bare Fe_3O_4, $Fe_{1-x}Mn_xFe_2O_4$ ($x = 0.15$ and 0.5) nanoparticles. The specific magnetization of $Fe_{1-x}Mn_xFe_2O_4$ ferrite particles initially increased with increasing Mn^{2+} concentration with 'x' up to a value of 65.9 emu/g for $x = 0.5$. This observation was well matched with the substituted ferrites reported by Bahadur et al. Anhysteric M–H curve without any detectable coercivity and remanence indicates a superparamagnetic behavior at room temperature for all samples. The entire curve showed perfect Langevin behavior without hysteresis. The saturation magnetization value (Ms) for $Fe_{0.5}Mn_{0.5}Fe_2O_4$ NPs was 65.9 emu/g while Ms for $Fe_{0.85}Mn_{0.15}Fe_2O_4$ and PMIDA–$Fe_{0.5}Mn_{0.5}Fe_2O_4$ nanoparticles were decreased to 52.11 emu/g and 44.33 emu/g respectively. The presence of organophosphono moiety on the surface of the modified nanoparticles leads to decrease of Ms compared to uncoated nanoparticles.

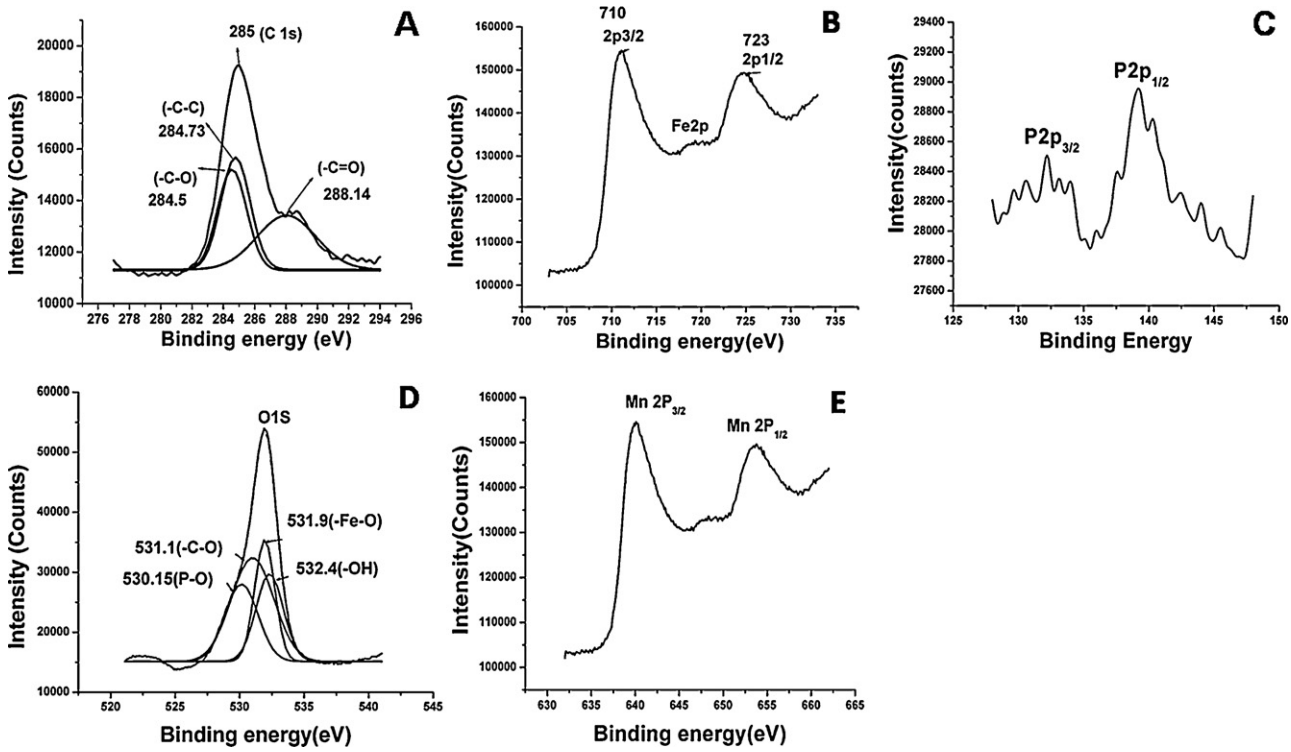

Fig. 4. High resolution ray photoelectron spectra of (A) C1s, (B) Fe2p, (C) P2p, (D) O1s, and (E) Mn2p of PMIDA–$Fe_{0.5}Mn_{0.5}Fe_2O_4$.

3.4. Peroxidase-like activity

It was already established that magnetite (Fe_3O_4) nanoparticles (MNPs) possess an intrinsic peroxidase-like catalytic activity towards the oxidative degradation of TMB in the presence of H_2O_2. This was aroused due to the heterogeneous Fenton like activity of surface Fe^{2+} atoms towards the degradation of hydrogen peroxide [13]. This catalytic property of MNPs was exploited previously to replace the conventional enzyme (HRP) used in ELISA [35]. It was previously observed that with the presence of doped Mn^{2+} in the magnetite structure, the Fenton like activity of the nanocomposites was enhanced and this enhancement strongly favored the hydrogen peroxide decomposition as well as organic dye oxidation. The rate of the decomposition reaction was also increased with the increasing Mn^{2+} concentration in the mixed ferrite nanoparticles [27,28]. This increased reactivity of Mn^{2+} doped mixed ferrites over bare magnetite could be envisaged due to the thermodynamically favorable single electron transfer reduction of Mn^{3+} by the surface Fe^{2+} ions as shown by the following reactions [27,42]:

$$Mn_{surf}{}^{2+} + H_2O_2 \rightarrow Mn_{surf}{}^{3+} + OH^- + \bullet OH \quad (2)$$

$$Fe^{2+} + Mn^{3+} \rightarrow Fe^{3+} + Mn^{2+}, \quad E^0 = 0.73\,V \quad (3)$$

This single electron reduction of Mn^{3+} by Fe^{2+} is feasible due to the higher reduction potential of Mn^{3+}/Mn^{2+} ($E^0 = 1.51$ V) compared to Fe^{3+}/Fe^{2+} ($E^0 = 0.77$ V). It was predicted that high conductivity of magnetite as a semiconductor nanoparticles [43,44] can catalyze the efficient regeneration of the surface Mn^{2+} species which would be responsible for the remarkably increased activity of nanoparticles for H_2O_2 decomposition and organic dye oxidation.

Inspired by these facts, the peroxidase-like behaviors of bare Fe_3O_4 as well as all these mixed ferrites were observed using TMB as a chromomeric substrate [45,46]. Fig. 6A represented the catalytic reaction of TMB using bare Fe_3O_4 as well as all these mixed ferrites after reaction for 25 min. In all the catalytic degradations of TMB, two peaks were observed at 369 and 652 nm, indicating that TMB was oxidized by our nanoparticles. Fig. 6B presented the time–course curves of the different reaction systems catalyzed by bare Fe_3O_4, $Mn^{II}{}_{0.15}Fe^{II}{}_{0.85}Fe^{III}{}_2O_4$, PMIDA–$Mn^{II}{}_{0.5}Fe^{II}{}_{0.5}Fe^{III}{}_2O_4$ and $Mn^{II}{}_{0.5}Fe^{II}{}_{0.5}Fe^{III}{}_2O_4$ nanoparticles within 25 min keeping catalyst as well as substrate concentration same. It was observed that the catalytic activity of MNPs towards TMB degradation displayed hyperbolic kinetics and the order was $Mn^{II}{}_{0.5}Fe^{II}{}_{0.5}Fe^{III}{}_2O_4$ > PMIDA–$Mn^{II}{}_{0.5}Fe^{II}{}_{0.5}Fe^{III}{}_2O_4$ > $Mn^{II}{}_{0.15}Fe^{II}{}_{0.85}Fe^{III}{}_2O_4$ > Fe_3O_4 respectively. This observation was comparable with the methylene blue oxidation by Mn^{2+} containing ferrites as reported by Lago et al. [27]. They observed that Mn^{2+} on the surface of mixed ferrites exhibited the possibility of forming redox couple Mn^{2+}/Mn^{3+}, aiming to produce hydroxyl radicals which can catalyze the oxidative

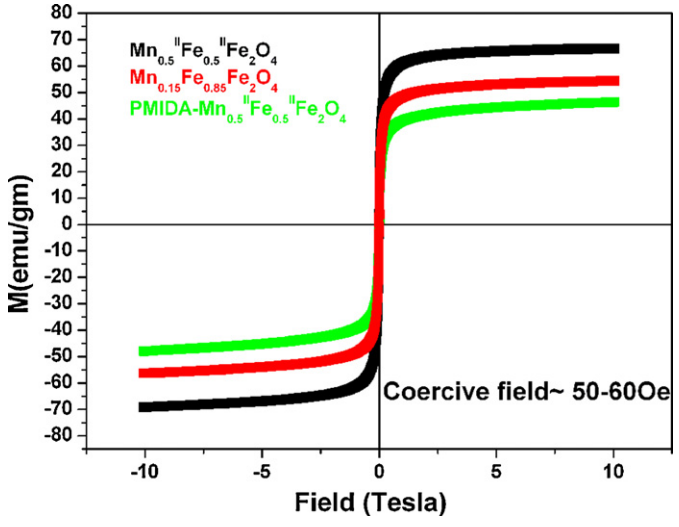

Fig. 5. Magnetization curves of (A) $Fe_{.85}Mn_{0.15}Fe_2O_4$, (B) $Fe_{0.5}Mn_{0.5}Fe_2O_4$, and (C) PMIDA–$Fe_{0.5}Mn_{0.5}Fe_2O_4$.

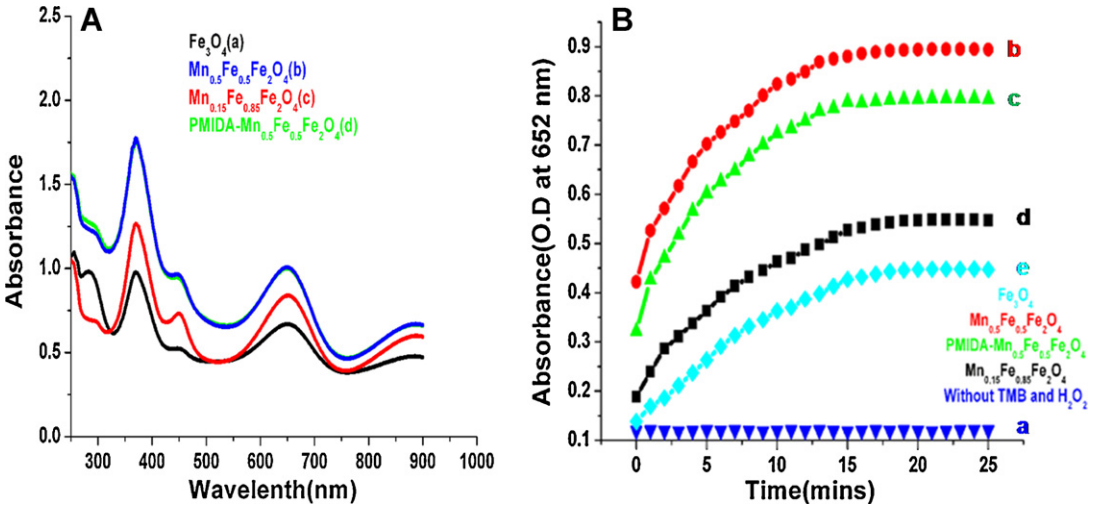

Fig. 6. (A) UV–vis absorption spectra of the TMB–H_2O_2 reaction system catalyzed by (a) Fe_3O_4, (b) $Fe_{0.5}Mn_{0.5}Fe_2O_4$, (c) $Fe_{0.85}Mn_{0.15}Fe_2O_4$, and (d) PMIDA–$Fe_{0.5}Mn_{0.5}Fe_2O_4$ for 25 min. (B) UV–vis absorption–time course curves of (a) a control for $Fe_{0.5}Mn_{0.5}Fe_2O_4$ in the same buffer without TMB–H_2O_2 and reaction system catalyzed by (b) $Fe_{0.5}Mn_{0.5}Fe_2O_4$ MNPs, (c) PMIDA–$Fe_{0.5}Mn_{0.5}Fe_2O_4$, (d) $Fe_{0.85}Mn_{0.15}Fe_2O_4$, and (e) Fe_3O_4.

degradation of TMB in H_2O_2. Based on the higher catalytic activity of $Mn^{II}_{0.5}Fe^{II}_{0.5}Fe^{III}_2O_4$ compared to previously discussed nanoparticles, $Mn^{II}_{0.5}Fe^{II}_{0.5}Fe^{III}_2O_4$ and PMIDA–$Mn^{II}_{0.5}Fe^{II}_{0.5}Fe^{III}_2O_4$ were chosen for the further kinetic analysis as well as immunoassay applications.

3.5. Steady state kinetics study

In order to authenticate the dependence of catalytic activity of the $Mn^{II}_{0.5}Fe^{II}_{0.5}Fe^{III}_2O_4$ on pH, temperature and substrate concentration, the peroxidase activity of $Mn^{II}_{0.5}Fe^{II}_{0.5}Fe^{III}_2O_4$ was evaluated with varying parameters similar with Fe_3O_4 and HRP respectively (Fig. 7A–C). Results revealed that the best catalytic activity of nanoparticle towards TMB oxidation was observed at pH 4 and 40 °C similar to the previous reports [13]. Thus, to investigate the mechanism of the peroxidase activity of $Mn^{II}_{0.5}Fe^{II}_{0.5}Fe^{III}_2O_4$ nanoparticles, pH 4 and 40 °C was adopted as the apparent steady-state kinetic parameters for the catalytic reaction. Apparent steady-state reaction rates at different concentrations of substrate were obtained by calculating the slopes of initial absorbance changes with time at a fixed concentration of catalyst. The oxidation of TMB catalyzed by $Mn^{II}_{0.5}Fe^{II}_{0.5}Fe^{III}_2O_4$ shown in Fig. 8A and B displayed typical Michaelis–Menten kinetics. The datas were fitted to the Michaelis–Menten model (curves shown in Fig. 8C–D) and the catalytic parameters were obtained (Table 2). The K_m value of the TMB degradation by $Mn^{II}_{0.5}Fe^{II}_{0.5}Fe^{III}_2O_4$ considering H_2O_2 as the substrate was significantly higher than that for HRP. This result concluded that a much higher concentration of H_2O_2 was required to obtain maximal reaction velocity for $Mn^{II}_{0.5}Fe^{II}_{0.5}Fe^{III}_2O_4$. The K_m value of the $Mn^{II}_{0.5}Fe^{II}_{0.5}Fe^{III}_2O_4$ with TMB as the substrate was comparatively lower than for HRP (Table 2), suggesting that the $Mn^{II}_{0.5}Fe^{II}_{0.5}Fe^{III}_2O_4$ have a considerably higher affinity for TMB than HRP. The K_{cat}/K_m value of the $Mn^{II}_{0.5}Fe^{II}_{0.5}Fe^{III}_2O_4$ compared to HRP considering TMB as substrate appeared significantly higher at the same concentration of nanoparticles and HRP. This enhancement was due to the lower K_m value of $Mn^{II}_{0.5}Fe^{II}_{0.5}Fe^{III}_2O_4$ taking TMB as a substrate. The K_{cat}/K_m value of the $Mn^{II}_{0.5}Fe^{II}_{0.5}Fe^{III}_2O_4$ with H_2O_2 as the substrate was significantly smaller than that for HRP, corresponding to the larger K_m value for H_2O_2. So it can be concluded that as a catalytic agent, $Mn^{II}_{0.5}Fe^{II}_{0.5}Fe^{III}_2O_4$ exhibits greater catalytic efficiency than HRP considering TMB as a substrate but lower efficiency for H_2O_2. The similar catalytic activity was generated due to the presence of a huge number of Mn^{2+} as well as Fe^{2+} ions on the surface, providing active sites for catalysis. It was also observed from Fig. 6B that the catalytic property of $Mn^{II}_{0.5}Fe^{II}_{0.5}Fe^{III}_2O_4$ was higher than the normal magnetite as reported by Yans group [13]. The catalytic power of our nanoparticles is even greater than the most advanced catalyst as reported by Gu et al. [26] which was predicted for the effect of Mn^{2+} substitution in the magnetite structure. As the catalytic activity also depends on the size of nanoparticles, it was also expected that so our 8–10 nm nanoparticles showed greater catalytic activity compared to 200 nm nanoparticles as reported by Gao et al. due to the combined effect of size and Mn^{2+} doping [35]. In general, the high catalytic efficiency of $Mn^{II}_{0.5}Fe^{II}_{0.5}Fe^{III}_2O_4$ was speculated due to (i) combined Fenton like activity of Fe^{2+} & Mn^{2+} ions in the $Mn^{II}_{0.5}Fe^{II}_{0.5}Fe^{III}_2O_4$ exhibiting a dominant role in the catalytic peroxidase like activity, (ii) higher surface area due to small size (iii) the strong affinity of two $-NH_2$ groups of TMB towards the surface of negatively charged PMIDA–$Mn^{II}_{0.5}Fe^{II}_{0.5}Fe^{III}_2O_4$ nanoparticles. (Zeta potential measured −35 to −39 mV.)

The dependence of peroxidase-like activity of $Mn^{II}_{0.5}Fe^{II}_{0.5}Fe^{III}_2O_4$ on the nanoparticle concentrations was established in Fig. 9. It was shown in the graph that there is a linear correlation between the absorbance with increasing $Mn^{II}_{0.5}Fe^{II}_{0.5}Fe^{III}_2O_4$ concentration indicating that the nanoparticles can be used as a mimic enzyme label in bioanalysis.

3.6. Detection of mouse IgG by PMIDA–$Mn^{II}_{0.5}Fe^{II}_{0.5}Fe^{III}_2O_4$ linked immunoassay

Encouraged by its peroxidase-like catalytic properties, we exploited the fabricated PMIDA–$Mn^{II}_{0.5}Fe^{II}_{0.5}Fe^{III}_2O_4$ in enzyme linked immunosorbent assay (Fig. 10) using mouse IgG as the detection analyte. PMIDA–$Mn^{II}_{0.5}Fe^{II}_{0.5}Fe^{III}_2O_4$ nanoparticles were selected for the immunoassay applications because of the amenable $-CO_2H$ groups on the surface which can be utilized for the immobilization with specific antibodies/biomolecules. The performance of PMIDA–$Mn^{II}_{0.5}Fe^{II}_{0.5}Fe^{III}_2O_4$ as a substitute for HRP was evaluated by both direct and indirect ELISA method. In both direct and indirect immunoassays protocol (Fig. 10A and B), the mouse IgG was directly immobilized on the microtiter plate wells through nonspecific interaction, and the PMIDA–$Mn^{II}_{0.5}Fe^{II}_{0.5}Fe^{III}_2O_4$ was functionalized with antimouse IgG/anti-goat IgG. From the results obtained (the results given in the graphs are the averages of three repetitive

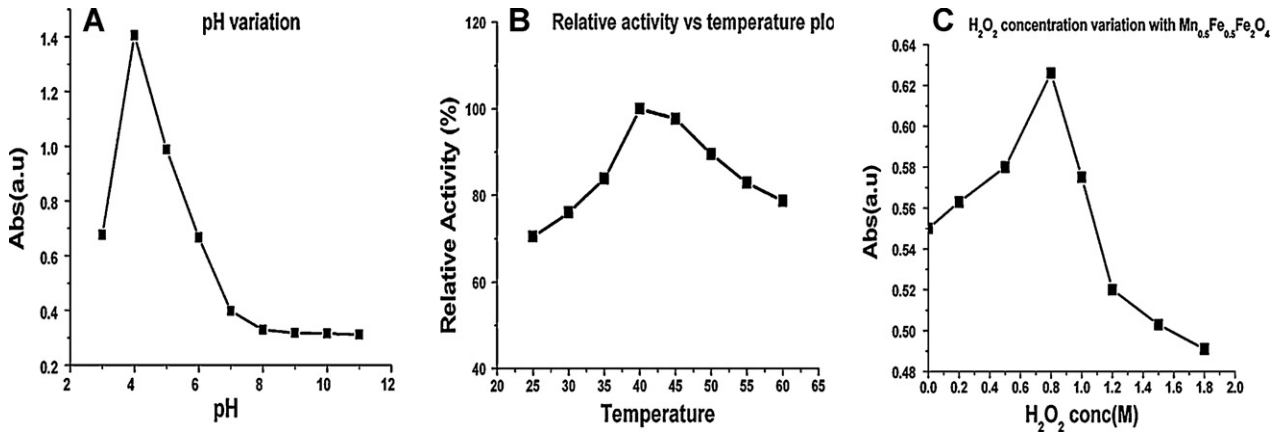

Fig. 7. The dependence of peroxidase-like activity of the $Fe_{0.5}Mn_{0.5}Fe_2O_4$ MNPs is pH, temperature, and H_2O_2 concentration.

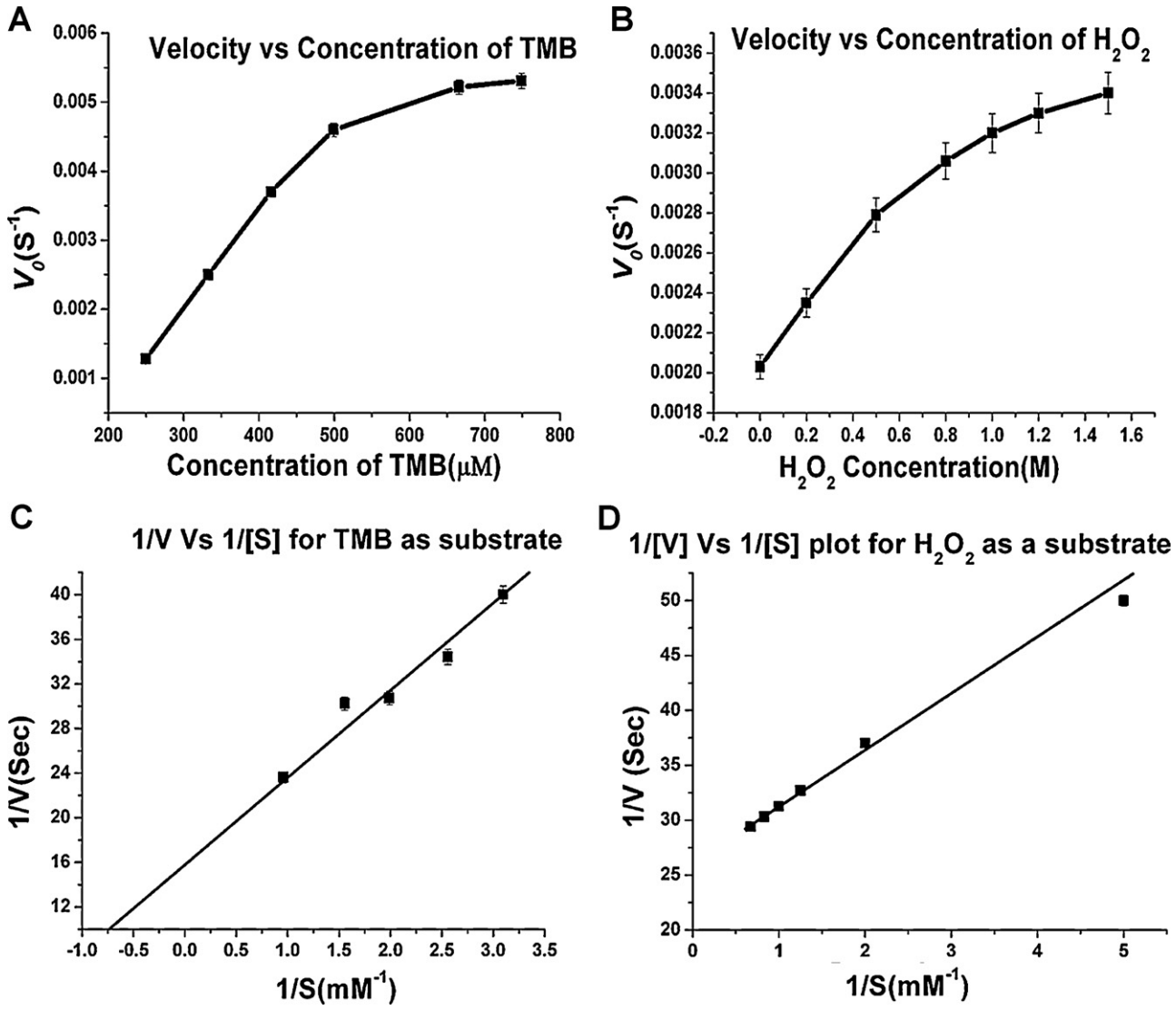

Fig. 8. Kinetic assay and catalytic mechanism for $Fe_{0.5}Mn_{0.5}Fe_2O_4$ with (A) TMB and (B) H_2O_2 as substrates, respectively. Error bars in the curves represent the standard error derived from three repeated measurements. (C) and (D) Double-reciprocal plots of activity of $Fe_{0.5}Mn_{0.5}Fe_2O_4$ MNPs at a fixed concentration of one substrate versus varying concentration of the second substrate for TMB and H_2O_2.

Table 2
Comparison of kinetic parameters of $Mn_{0.5}Fe_{0.5}Fe_2O_4$ and HRP. [E] is nanoparticle and HRP concentration, K_m is the Michaelis constant, V_{max} is the maximal reaction velocity and K_{cat} is the catalytic constant, where $K_{cat} = V_{max}/[E]$. Here K_{cat} value shows the catalytic efficiency per nanoparticle. (These data is the average of three repetitive measurements.) The values of HRP were taken from the previous standard reports [13].

	[E] (M)	Substrate	K_m (mM)	V_{max} (MS^{-1})	K_{cat} (S^{-1})	K_{cat}/K_m ($M^{-1}\,S^{-1}$)
MNP	3.2×10^{-10}	TMB	0.139 ± 0.02	4.5×10^{-6}	1.4062×10^{4}	10.1165×10^{7}
	3.2×10^{-10}	H_2O_2	310 ± 0.01	3.63×10^{-6}	1.134×10^{4}	3.65×10^{4}
HRP	2.5×10^{-11}	TMB	0.434	10×10^{-8}	4×10^{3}	9.2×10^{6}
	2.5×10^{-11}	H_2O_2	3.7	8.71×10^{-8}	3.48×10^{3}	9.4×10^{5}

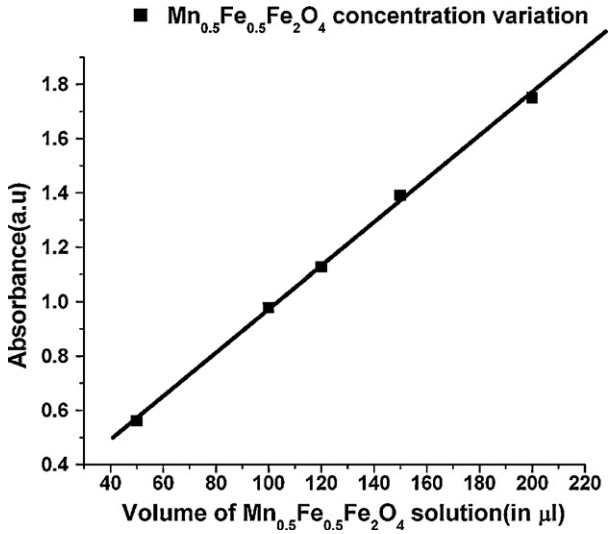

Fig. 9. Concentration dependency of peroxidase-like activity for $Fe_{0.5}Mn_{0.5}Fe_2O_4$ in presence of H_2O_2 and TMB.

configurations), a significant correlation was noticed between the concentrations of the mouse IgG with the detected absorbance values. The correlation coefficient obtained were 0.9981 and 0.9942 (Fig. 10A and B) and this suggesting that peroxidase mimetics PMIDA–$Mn^{II}_{0.5}Fe^{II}_{0.5}Fe^{III}_2O_4$ could efficiently detect the amount of mouse IgG immobilized at titre plates. The data of Fig. 10A and B specified a detection limit of 0.1 μg/ml and the linear range of our biodetection probe was found from 0.1 μg/ml to 2.2 μg/ml. The linear increase of the absorbance as a function of IgG concentration corroborated the significance for biological detection by our synthesized immunoassay toolbox. The detection limit obtained in our PMIDA–$Mn^{II}_{0.5}Fe^{II}_{0.5}Fe^{III}_2O_4$ modified immunosorbent assay was found to be superior as compared to the method reported by Gu et al. [26].

It was also assumed that the amenable carboxyl groups in PMIDA provide convenient sites for linkage with IgGs to the MNPs through linking their amino groups using covalent conjugation. As a demonstration, we functionalized the PMIDA–$Mn^{II}_{0.5}Fe^{II}_{0.5}Fe^{III}_2O_4$ nanoparticles with anti-mouse IgG. A back ELISA protocol was established to estimate the concentration of residual IgG after binding to nanoparticles (Fig. S3). It was observed that approximately 32% of the antibodies were immobilized on MNPs by using the current experimental procedure.

3.7. Bioseparation of FITC-rabbit anti goat IgG using PMIDA–$Mn^{II}_{0.5}Fe^{II}_{0.5}Fe^{III}_2O_4$

In order to evaluate the efficiency of PMIDA–$Mn^{II}_{0.5}Fe^{II}_{0.5}Fe^{III}_2O_4$ for magnetic-bioseparation of FITC-rabbit-anti-goat IgG, the antigens were attached to the surface of the MNPs through the covalent conjugation between the available NH_2 groups of the antigens and the activated carboxyl groups on the nanoparticle surface. This antigen labeled MNPs were further used in the magnetic separation and detection of FITC-antigen. Based on the specific antigen–antibody interaction between FITC-anti-goat IgG and goat-IgG labeled MNPs, FITC-anti-goat IgG was magnetically concentrated and separated from the solution. Fig. 11A showed the fluorescence spectra of the free antibody, the PMIDA-linked anti-goat IgG nanocomposites solution, the supernatant after the magnetic separation and PMIDA-nanocomposites (unmodified) respectively. As compared to the free antibody, the fluorescence of the supernatant was very weak while that of the nanocomposites solution was very strong; corroborating that FITC-anti-goat IgG was bound to the antibody

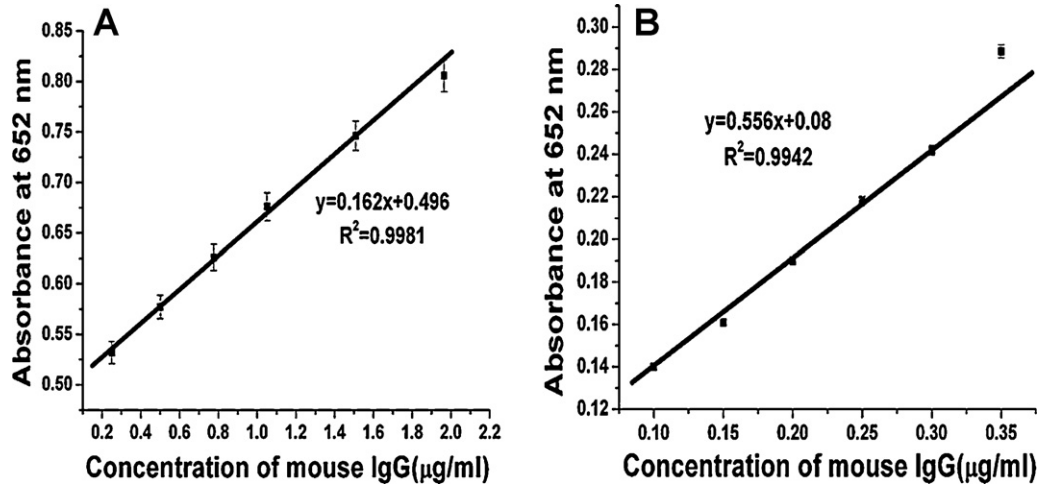

Fig. 10. Results of PMIDA–$Fe_{0.5}Mn_{0.5}Fe_2O_4$-linked immunosorbent assay for detection of (A) mouse IgG as a model analyte using the direct (B) mouse IgG as a model analyte using indirect ELISA configurations respectively. Error bars shown represent the standard error derived from three repeated measurements.

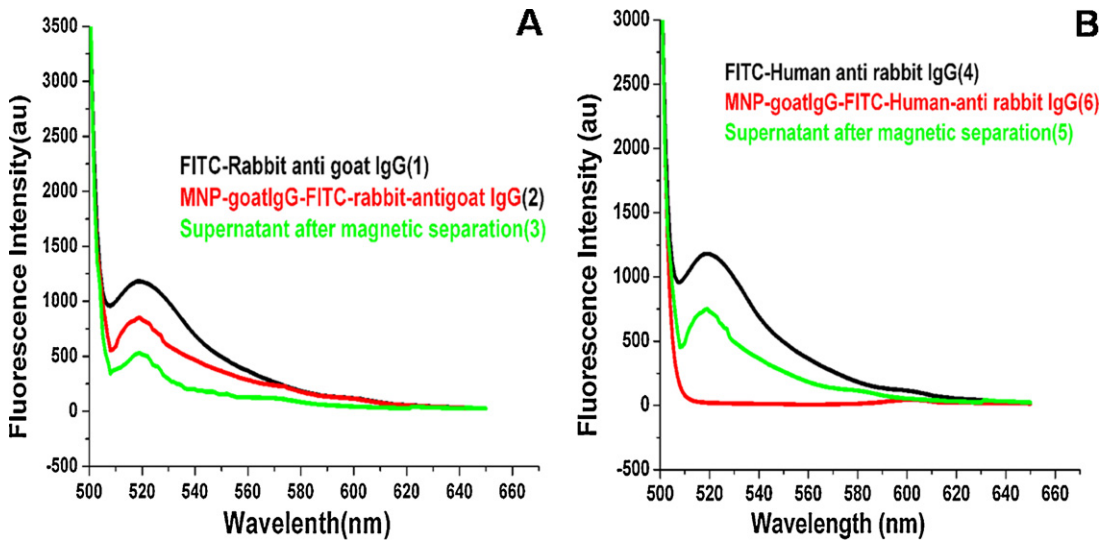

Fig. 11. Representations of fluorescence spectra of the immunoassay systems (A) target experiment performed using FITC-rabbit anti-goat IgG and goat-anti mouse IgG system: (1) FITC-labeled rabbit anti-goat IgG solution, (2) PMIDA–$Mn_{0.5}Fe_{0.5}Fe_2O_4$-goat-IgG-FITC-rabbit IgG, and (3) supernatant solution after magnetic separation. (B) Control experiment based on the FITC-rabbit anti-human IgG and goat-antimouse IgG system: (4) FITC-rabbit anti-human IgG solution, (5) supernatant solution after magnetic separation, (6) PMIDA–$Mn_{0.5}Fe_{0.5}Fe_2O_4$-goat-IgG-FITC-rabbit anti human IgG.

linked nanocomposites and got separated [37]. Fig. 11B showed the selectivity of the magnetic separation method, testified by the control experiment following a similar strategy. In brief, the antibody used for magnetic bio-separation in the control experiment was FITC-labeled rabbit antihuman IgG antibody instead of the anti-goat antibody. The fluorescence intensity of the supernatant was virtually unchanged after the magnetic separation. Meanwhile, the magnetic nanoparticle solution hardly exhibited any fluorescence, which revealed that FITC-rabbit-anti-human IgG was not bound to the antibody modified magnetic nanoparticles. The results demonstrated the excellent selectivity of the present magnetic bio-separation technology based on the carboxyl functionalized MNPs.

4. Conclusions

In a nutshell, a series of $Mn^{II}_xFe^{II}_{1-x}Fe^{III}_2O_4$ nanoparticles were synthesized by a simple and cheap method and possessed intrinsic peroxidase-like catalytic activity under harsh conditions. It was thoroughly observed that the peroxidase activity was enhanced as a function of Mn^{2+} concentration and showed typical Michaelis–Menten kinetics exhibiting higher efficiency compared to Fe_3O_4 nanoparticles. Furthermore, these nanoparticles can play the role of novel enzyme mimetics exhibiting higher K_{cat} value compared to magnetite nanoparticles. Exploiting the enhanced peroxidase properties, a modified immunoassay was employed for the detection of IgGs using PMIDA–$Mn^{II}_{0.5}Fe^{II}_{0.5}Fe^{III}_2O_4$ nanoparticles, mimicking the typical role of HRP utilized in ELISA. The results showed better efficacy exhibiting lower detection limit (0.1 μg/ml) of mouse IgG compared to previous reports and this detection level was ten times lower than previous reports of magnetite-linked ELISA. By employing the combined magnetism and functionalities on antibody labeled PMIDA–$Mn^{II}_{0.5}Fe^{II}_{0.5}Fe^{III}_2O_4$ nanoparticles, this system showed efficacy as a potential analytical tool for the magnetic bioseparation as well as detection of FITC-labeled rabbit IgG. Stimulated by the positive attributes of the low detection limit, cost effectiveness, enhanced selectivity, we expect that this method will be a promising multifunctional tool for enzyme mimetics, catalysis, biodetection and bioseparation.

Acknowledgements

The authors gratefully acknowledge Dr. K.R. Patil, Centre of Material Characterization, National Chemical Laboratory (NCL), Pune, for assistance with the XPS studies. Authors are grateful to the Council of Scientific and Industrial Research (CSIR), New Delhi, for providing financial support for this work. Authors are also grateful to Dr Soma Das, Department of Physics, Univerisity of Aveiro, Portugal for VSM analysis.

Appendix A. Supplementary data

Supplementary data associated with this article can be found, in the online version, at doi:10.1016/j.talanta.2011.09.026.

References

[1] M. Brahler, R. Georgieva, N. Buske, A. Muller, S. Muller, J. Pinkernelle, U. Teichgraber, A. Voigt, H. Banmler, Nano Lett. 6 (2006) 2505.
[2] M.C. Denis, U. Mahmood, C. Benoist, D. Mathis, R. Weissleder, Proc. Natl. Acad. Sci. 101 (2004) 12634.
[3] J.W. Bulte, Methods Mol. Med. 124 (2006) 419.
[4] M. Hoehn, U. Himmelreich, J. Magn. Reson. Imaging 27 (2008) 941.
[5] C. Burtea, S. Laurent, A. Roch, L. Vander Elst, R.N. Muller, J. Inorg. Biochem. 99 (2005) 1135.
[6] S. Boutry, S. Laurent, L. Vander Elst, R.N. Muller, Contrast Media Mol. Imaging 1 (2006) 15.
[7] J.M. Perez, F.J. Simeone, A. Tsourkas, L. Josephson, R. Weissleder, Nano Lett. 4 (2004) 119.
[8] B.M. Oscar, P.M. Maria, T. Pedro, R.C. Jesus, B. Pierre, S. Martin, X.Q. Zhao, V.V. Sabino, Biomaterials 26 (2005) 5695.
[9] J.J. Cheng, B.A. Teply, S.Y. Jeong, C.H. Yim, D. Ho, I. Sherifi, S. Jon, O.C. Farokhzad, A.R. Khademhosseini, S. Langer, Pharm. Res. 23 (2006) 557.
[10] H. Tanaka, T. Sugita, Y.J. Yasunaga, S.J. Shimose, M. Deie, T. Kubo, T. Murakami, M. Ochi, J. Biomed. Mater. Res. Part A 73A (2005) 255.
[11] M.L. Matteucci, G. Anyarambhatla, G. Rosner, C. Azuma, P.E. Fisher, M.W. Dewhirst, D. Needham, D.E. Thrall, Clin. Cancer Res. 6 (2000) 3748.
[12] I.J. Majoros, A. Myc, T. Thomas, C.B. Mehta, J.R. Baker, Biomacromolecules 7 (2006) 572.
[13] L.Z. Gao, J. Zhuang, L. Nie, J. Zhang, Y. Zhang, N. Gu, T.H. Wang, J. Feng, D.L. Yang, S. Perrett, X.Y. Yan, Nat. Nanotechnol. 2 (2007) 577.
[14] H. Wei, E.K. Wang, Anal. Chem. 80 (2008) 2250.
[15] B. Teste, J. Vial, S. Descroix, T. Georgelin, J.M. Siaugue, J. Petr, A. Varenne, M.C. Hennion, Talanta 81 (2010) 1703.
[16] J. Zhao, G. Li, B. Wang, W. Liu, T. Nan, Z. Zhai, Z. Li, Q. Li, Anal. Bioanal. Chem. 386 (2006) 1735.

[17] C. Hempen, S.M. Leeuwen, H. Luftmann, U. Karst, Anal. Bioanal. Chem. 382 (2005) 234.
[18] A. Ambrosi, F. Airo, A. Merkoc, Anal. Chem. 82 (2010) 1151.
[19] M. Tudorache, A. Tencaliec, C. Bala, Talanta 77 (2008) 839.
[20] M. Varshney, L. Yang, X.L. Su, Y. Li, J. Food Prot. 68 (2005) 1804.
[21] Y. Jing, L.R. Moore, P.S. Williams, J.J. Chalmers, S.S. Farag, B. Bolwell, M. Zborowski, Biotechnol. Bioeng. 96 (2007) 1139.
[22] H.Y. Tsai, C.F. Hsu, I.W. Chiu, C.B. Fuh, Anal. Chem. 79 (2007) 8416.
[23] J.E. Smith, C.D. Medley, Z. Tang, D. Shangguan, C. Lofton, W. Tan, Anal. Chem. 79 (2007) 3075.
[24] F. Yu, Y. Huang, A. Cole, V.C. Yang, Biomaterials 30 (2009) 4716.
[25] P. Lahiri, S.K. Sengupta, J. Chem. Soc., Faraday Trans. 91 (1995) 3489.
[26] X.Q. Zhang, S.W. Gong, Y. Zhang, T. Yang, C.Y. Wang, N. Gu, J. Mater. Chem. 20 (2010) 5110.
[27] R.C.C. Costa, M.F.F. Lelis, L.C.A. Oliveira, J.D. Fabris, J.D. Ardisson, R.R.V.A. Rios, C.N. Silva, R.M. Lago, J. Hazard. Mater. 129 (2006) 171.
[28] P. Lahiri, S.K. Sengupta, ChemInform 69 (1991) 33.
[29] T.D. Nguyen, N.H. Phan, M.H. Do, K.T. Ngo, J. Hazard. Mater. 185 (2011) 653.
[30] X. Liang, S. Zhu, Y. Zhong, J. Zhu, P. Yuan, H. He, J. Zhang, Appl. Catal. B: Environ. 97 (2010) 151.
[31] S. Yang, H. He, D. Wu, D. Chen, X. Liang, Z. Qin, M. Fan, J. Zhu, P. Yuan, Appl. Catal. B: Environ. 89 (2009) 527.
[32] S. Rothbart, E. Ember, R.V. Eldik, Dalton Trans. 39 (2010) 3264.
[33] A. Xu, H. Xiong, G. Yin, J. Phys. Chem. A 113 (2009) 12243.
[34] H. Yingping, L. Xiangling, F. Yanfen, W. Qi, L. Kingtong, Wuhan Univ. J. Nat. Sci. 14 (2009) 262.
[35] L. Gao, J. Wu, S. Lyle, K. Zehr, L. Cao, D. Gao, J. Phys. Chem. C 112 (2008) 17357.
[36] J. Giri, P. Pradhan, V. Somani, H. Chelawat, S. Chhatre, R. Banerjee, D. Bahadur, J. Magn. Magn. Mater. 320 (2008) 724.
[37] L. Wang, J. Bao, L. Wang, F. Zhang, Y. Li, Chem. Eur. J. 12 (2006) 6341.
[38] L.C.A. Oliveira, R.M. Lago, R.V.R.A. Rios, R. Augusti, P.P. Sousa, W.N. Mussel, J.D. Fabris, Stud. Surf. Sci. Catal. 130 (2000) 2165.
[39] R.V. Upadhyay, K.J. Davies, S. Wells, S.W. Charles, J. Magn. Magn. Mater. 132 (1994) 249.
[40] M. Das, D. Mishra, P. Dhak, S. Gupta, T.K. Maiti, A. Basak, P. Pramanik, Small 5 (2009) 2883.
[41] J. Gao, S.Y. Dai, T.K. Li, Phys. Rev. B 67 (2003) 153403.
[42] R.C.C. Costa, M.D. Fatima, F. Lelis, L.C.A. Oliveira, J.D. Fabris, J.D. Ardisson, R. Rios, C.N. Silva, R.M. Lago, Catal. Commun. 4 (2003) 525.
[43] A.J. Bard, J.K. Leland, J. Phys. Chem. 91 (1987) 5076.
[44] A.F. White, Rev. Miner. 23 (1990) 467.
[45] S. Savard, P.D. Josephy, Mutagenesis 2 (1987) 97.
[46] P.D. Josephygg, T. Elingg, R.P. Mason, J. Biol. Chem. 257 (1982) 3669.